Revista Mexicana de Astronomía y Astrofísica, **49**, 3–10 (2013)

MILLIMETER AND SUBMILLIMETER COUNTERPARTS OF THE 2009 SEPTEMBER 26 SOLAR PROMINENCE

J. E. Pérez-León,[1] D. Hiriart,[1] and J. E. Mendoza-Torres[2]

Received 2012 June 27; accepted 2012 August 29

RESUMEN

Presentamos observaciones en longitudes de onda milimétricas y submilimétricas de una prominencia solar extendida. Los datos fueron obtenidos en el *Solar Submillimeter Telescope* (SST) durante observaciones rutinarias el 29 de septiembre de 2009. Las radio señales fueron detectadas a 1.41 mm (212 GHz) y 0.74 mm (405 GHz) durante un barrido de este a oeste realizado sobre el disco solar. La detección fue confirmada por medio de la imagen de He II del *Extreme Ultraviolet Imaging Telescope* del *Solar and Heliospheric Observatory* (EIT/SOHO). Los máximos de las temperaturas de brillo a 1.41 mm y 0.74 mm están separados por ∼4 minutos de arco y la emisión a 0.74 mm es más cercana al limbo solar. Suponiendo un mecanismo de emisión del tipo libre-libre, ambos máximos corresponden a un exceso en la temperatura de brillo de $T_b \sim 2 \times 10^3$ K, consistente con una temperatura y densidad electrónica de $T_e \sim 5.6 \times 10^3$ K y $n_e \sim 10^{10}$ cm^{-3}, respectivamente.

ABSTRACT

We present observations of the millimeter and submillimeter wavelength radio emission from an extended solar prominence. The data were obtained at the Solar Submillimeter Telescope (SST) during regular observations on 2009 September 26. The prominence signals were detected at 1.41 mm (212 GHz) and 0.74 mm (405 GHz) in an east-west raster practiced on the solar disk. Detection was confirmed by the He II image from the Extreme Ultraviolet Imaging Telescope of the Solar and Heliospheric Observatory (EIT/SOHO). The peak brightness temperature at the 1.41 mm and 0.74 mm are separated by ∼4 arcmin with the 0.74 mm one closer to the solar limb. Assuming a free-free emission mechanism, both peak intensities correspond to an excess of brightness temperature of $T_b \sim 2 \times 10^3$ K and they are consistent with an electron temperature and density of $T_e \sim 5.6 \times 10^3$ K and $n_e \sim 10^{10}$ cm^{-3}, respectively.

Key Words: Sun: filaments, prominences — Sun: radio radiation — Sun: UV radiation

1. INTRODUCTION

Solar prominences are large magnetic structures in the solar corona that confine a relatively cool ($T \sim 10^4$ K) and dense ($n_e \sim 10^9 - 10^{11}$ cm^{-3}) plasma. They have been successfully detected in several radio wavelengths from 167 MHz (Wild & Zirin 1956) to the millimetric region (Lantos & Raoult 1980; Apushkinskii & Topchilo 1985; Golubchina et al. 2009). Some of these observations were made during solar eclipses obtaining a large signal to noise ratio when the emission from the quiet Sun was blocked by the Moon. From radio wavelength observations, it has been estimated that solar prominences had altitudes over the chromosphere level of 3×10^{10} cm (Jejčič & Heinzel 2007) and $25 \pm 5 \times 10^8$ cm (Apushkinskii & Topchilo 1985; Apushkinskij et al. 1996). Other solar prominence parameters such as the electron density and temperature, as well as its bulk and micro-turbulent velocity, have been computed and reported in the literature from observations using radio waves. However, observational data of solar active regions at

[1]Instituto de Astronomía, Universidad Nacional Autónoma de México, Ensenada, B.C., Mexico.

[2]Instituto Nacional de Astrofísica, Óptica y Electrónica, Tonantzintla, Puebla, Mexico.

millimeter and submillimeter wavelengths are scarce because of the unpredictable nature of the eruptive solar activities (such as flares and prominences) and the very few dedicated solar radio telescopes operating at those wavelengths. These observations are more complicated when the active region is seen projected on the solar disk since the quiet Sun background emission makes them difficult. A better situation is obtained when a prominence is observed out of the projected solar disk.

In this paper we present the results of the millimeter and submillimeter emission observations of the solar prominence located at $\phi = +45°$ over the north-east solar limb at 19:19 UT on 2009 September 26. We compare the radio observations to the full disk chromospheric images from the Extreme Ultraviolet Imaging Telescope of the Solar and Heliospheric Observatory (hereafter EIT/SOHO). The aim of this work is to contribute to the solar prominence observational data in the centimeter and submillimeter bands.

This paper is organized as follows: in § 2 the instrumentation and observations are presented; the process of data reduction is explained in § 3; the results of the observations and the comparison to the UV observations of the EIT/SOHO are presented in § 4; in § 5 we discuss the results and compute the prominence brightness temperature, the plasma electron temperature and the density, following the formalism of Dulk (1985) applied to the emission near 1 mm; finally, in § 6 we present the conclusions of this work.

2. OBSERVATIONS

Observations near 1 mm were made at the Solar Submillimeter Telescope (SST). The SST is a single Cassegrain antenna of 1.5 meters diameter enclosed inside a protective radome; it is completely devoted to study the Sun at millimeter and submillimeter wavelengths. It is located at *Complejo Astronómico El Leoncito* (CASLEO), San Juan, Argentina Andes, at an elevation of 2552 meters above mean sea level. A detailed description of the SST can be found in Kaufmann et al. (2008).

The SST has six independent non-cryogenic total power receivers, each of them having their own feed horn and heterodyne section. Four of them are tuned at a wavelength of 1.41 mm (212 GHz) and two at 0.74 mm (405 GHz). The receivers bandwidth is $\Delta f = 1$ GHz and the measurement time resolution is 1 ms, providing a sensitivity of ∼3 K. Figure 1 shows the footprint of the six beam receivers projected on the solar disk. Four beams (1 to 4) correspond to the 1.41 mm receivers and have a half power beam

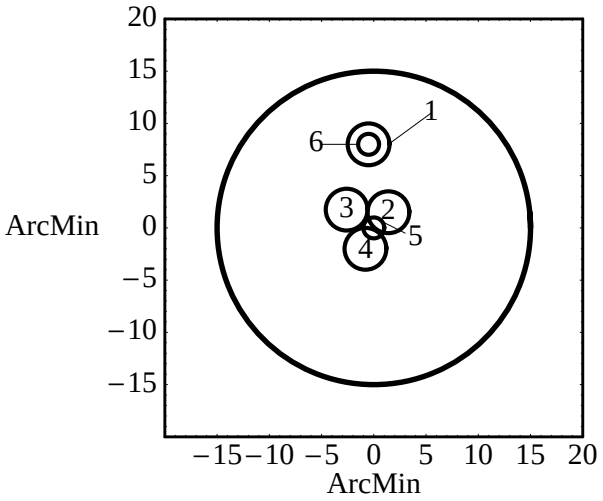

Fig. 1. SST footprint of the beam receivers projected on the solar disk. Beam 5 is located on the optical axis of the radio telescope. The receivers used for the observations in this paper are the two concentric beams 1 & 6: beam 1 for the 1.41 mm receiver and beam 6 for the 0.74 mm receiver (Kaufmann et al. 2008).

width (HPBW) of ∼4′. Two beams (5 and 6) correspond to the 0.74 mm receivers and have a HPBW of ∼2′. The beam configuration is such that beam 5 is located on the optical axis of the telescope. A cluster of three beams at 1.41 mm (2, 3, and 4) is located near the optical axis of the telescope, with beams 2 and 4 partially overlapping the footprint of beam 5. Beams 1 and 6 are separated by ∼6 arcsec from the central beam cluster and provide a reference of the background Sun emission at the two observing frequencies. These last two beams and they associated receivers at 1.41 and 0.74 mm, respectively, were used in raster mode of the telescope to detect the solar prominence.

During radio observations, the SST employs several calibration routines to determine the noise temperature of the receivers, $T_{\rm RX}$, and the atmospheric zenith opacity, τ_0, at the observing frequencies. The receiver noise temperature is easily computed taking into account the measurements of the analog to digital count values (ADC) $\bar{Z}_{\rm L}$ and $\bar{Z}_{\rm H}$ made from the ambient, $T_{\rm L}$, and hot-temperature, $T_{\rm H}$, calibration loads, respectively. These measurements are expressed as

$$\bar{Z}_{\rm L} = \beta(T_{\rm L} + T_{\rm RX})\,, \qquad (1)$$

and

$$\bar{Z}_{\rm H} = \beta(T_{\rm H} + T_{\rm RX})\,, \qquad (2)$$

where β relates the measurements to the physical temperatures. These equations can be easily solved

for β and $T_{\rm RX}$. To calculate τ_0, the SST makes a continuous vertical scan for elevations in the range of $5^\circ < z < 85^\circ$. The measured values at each elevation are related to the elevation angle z by (Hiriart et al. 1997; Otárola, Hiriart, & Pérez-León 2009)

$$\ln(\bar{Z}_{\rm L} - \bar{Z}(z)) = -\tau_0 \csc(z) + \ln(\beta T_{\rm L})\,. \qquad (3)$$

Thus, the solar radiation, represented by a brightness temperature T_b, after passing through the atmosphere produces an observed signal, $T_{\rm OBS}$, given by

$$T_{\rm OBS} = \eta\, T_b\, e^{-\tau_0/\sin z}\,, \qquad (4)$$

where η is the corresponding beam efficiency. The SST beam efficiencies are reported in Silva et al. (2005).

The SST has an alt-azimuth mount and it is covered by a radome that allows the pass of electromagnetic radiation in the millimeter and submillimeter wavelength range. Therefore, calibration of the telescope pointing has to be done with the kind of radiation available to the detectors. To localize more precisely the Sun center, the telescope made rasters on the sky. On 2009 September 26 (at 19:19 UT) one of these rasters occurred during the appearance of the solar prominence allowing its detection by the telescope receivers. This prominence was also detected by the EIT/SOHO telescope and images were available in four UV wavelengths (171, 195, 284, and 304 Å) corresponding to emission of radiation from highly ionized Fe and He II. We used UV observations from EIT/SOHO to complement the information provided by the millimeter and submillimeter wavelengths of the solar prominence.

The SST rasters are made with azimuthal (x-axis) scans and parallel along the elevation (y-axis) of the horizon coordinate system of the radio telescope. The raster x-range is from -40 to $+40$ arcmin and the raster y-range is from -30 to $+30$ arcmin, both relative to center of the solar disk. Each raster consists of 28 parallel scans spaced approximately by 2 arcmin, from which only 16 of then passed over the solar disk, taking approximately two points per arcmin. Once the rasters of the Sun surface were corrected for the rotation field effect of the SST (see § 3), the prominence was located at $\phi = +45^\circ$ over the East limb of the EIT/SOHO images on 2009 September 26 at about 19.19 UT.

Figure 2 presents one scan which runs on the x-axis over the local northern half part of the solar disk overlaid on a EIT/SOHO image. The solid line in the figure is the corresponding profile at 212 GHz as a function of the azimuth offset position relative to the center of the solar disk for the scan presented in the figure. The EIT/SOHO He II image corresponds to $\lambda = 30.4$ nm. Such emission is consistent with a temperature $T \sim 10^4$ K in accordance with the temperature stratification of the solar atmosphere. The emission in the EIT/SOHO image comes from the lowest chromospheric levels, which is the same region from where the high frequency radio-waves, such as the ones observed by the SST, are emitted. The solar prominence was revealed only in the He II image of the EIT/SOHO.

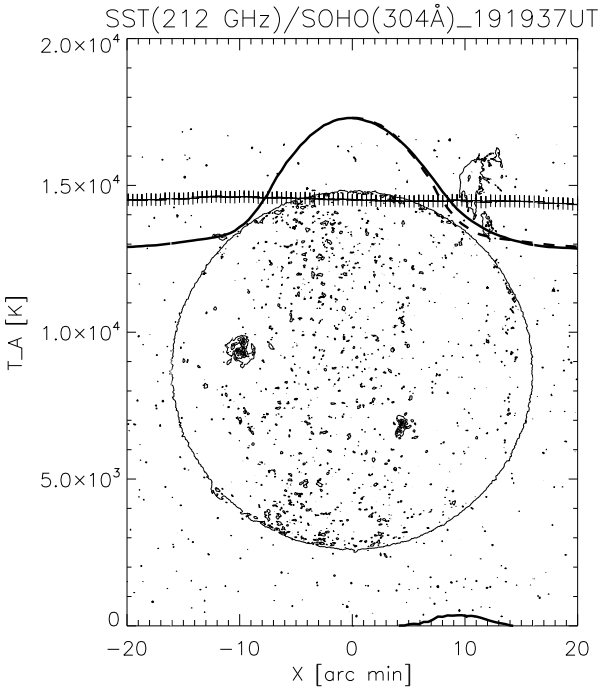

Fig. 2. One west-east scan of the SST over the solar disk. Crosses outline the scan trajectory over the He II image from EIT/SOHO. This scan runs at $y = +15.1$ arcmin relative to solar disk center. The continuous solid line, ranging from 1.5×10^4 to $\sim 2.2 \times 10^4$ on the y-axis, represents the corresponding signal profile at 212 GHz of antenna temperature vs. azimuth offset position relative to the solar disk center. The dashed line is the same scan pivoted around the coordinate $x = 0$ and projected on the former one. The difference between these two curves is a signal excess indicated by the solid line at the bottom of the graph at around $x = +10$ arcmin.

On the right half side of Figure 2 (west), beyond the solar limb, a notable feature breaks the monotonic decrement of the solar radiation profile respect to left (east) half of the scan. An examination of the EIT/SOHO images at the time of the scan indicates the presence of a solar prominence at the same location. Figure 3 presents the four UV images from

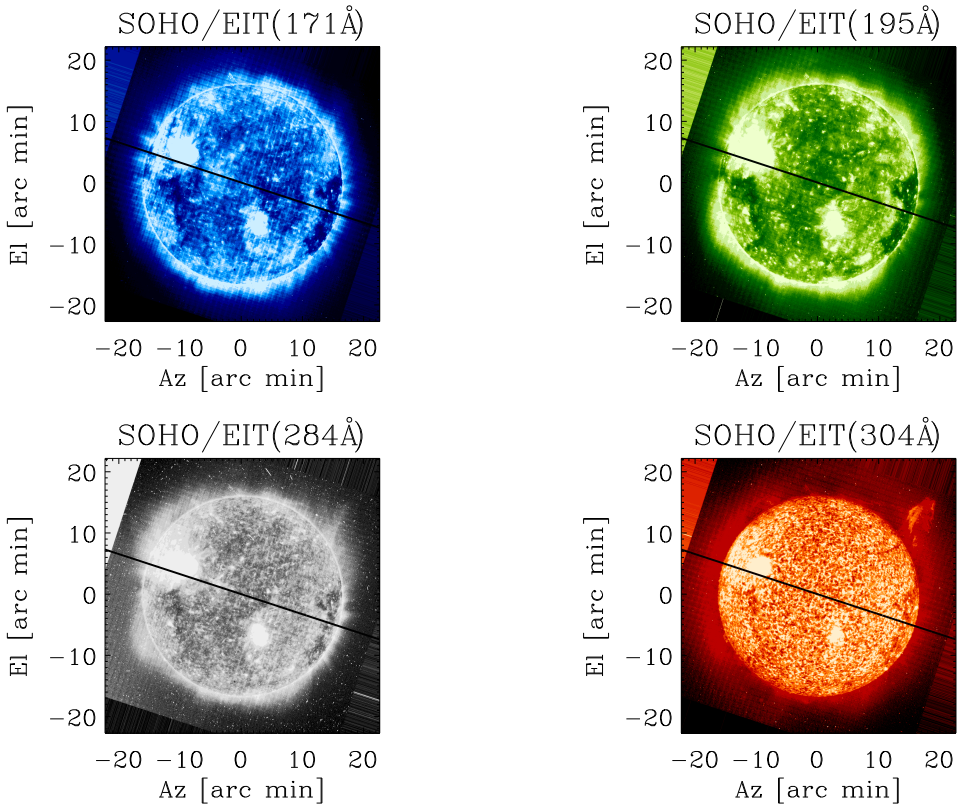

Fig. 3. Solar images by the EIT/SOHO at all its UV bands on 2009 September 26 at about 19:00 UT. The solar prominence is clearly shown in the image at 304 Å (bottom right corner), and it is marginally evident at 284 Å (bottom left corner). Presence of the prominence it is not evident either at 195 Å or at 171 Å images. From temperature models of the solar atmosphere, the image at 304 Å reveals the lowest chromospheric levels. The black solid line represents the solar P-angle with North on the right. The color figure can be viewed online.

the EIT/SOHO at the time of the SST observations. The solar prominence was revealed only in the He II image of the EIT/SOHO, so we proceeded with further data reduction of the SST data.

3. DATA REDUCTION

To correlate the SST scan observations to the EIT/SOHO images, two corrections were applied. First, rotations of the EIT/SOHO image were implemented according to the hour angle at the current observing time and the solar P-angle. Second, after image rotation, the raster was centered on the solar disk by evaluating the limb signal of selected scans using the method of Lindsey & Roellig (1991), which is explained as follows: theoretically, the SST scan profile should have an abrupt variation through the solar limb which may be crudely approximated by a Heaviside function. In a more realistic scenario, the scan has a *virtual* discontinuity which is a smoothed version of the Heaviside function that includes the convolution effects between the sharpness of the solar limb and the telescope beam. A point x_0 inside this *virtual* discontinuity is selected as a symmetry point which divides the virtual discontinuity into two symmetric halves. The symmetric point x_0 is determined with the help of the symmetric function T_s defined by

$$T_s \equiv \frac{1}{2}[T(x - x_0) + T(x + x_0)]\,, \qquad (5)$$

where T is the SST antenna temperature. Figure 4 shows the function T_s plotted for three distinct x_0 values. When the selected point is not the symmetry point of the *virtual* discontinuity, the function T_s spikes out. Only when x_0 is the symmetry point T_s will have a smooth behavior along the virtual discontinuity.

Thus, each scan will possess two symmetry points on each side of the solar disk, namely x_- and x_+. These points are not symmetrically located about the elevation axes of the solar disk; thus the sym-

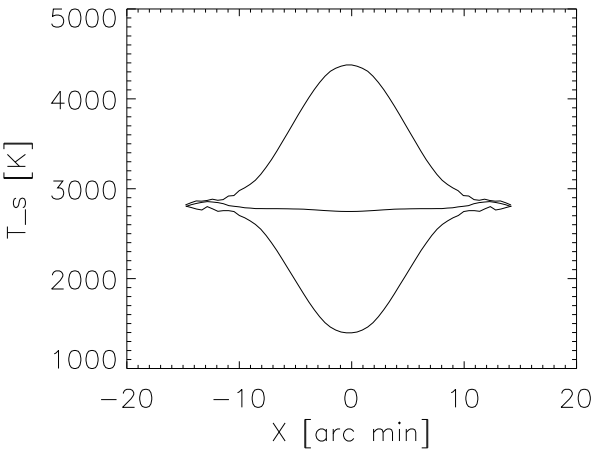

Fig. 4. The symmetric function T_s plotted for three different choices of the symmetry point x_0. Here the optimum choice of x_0 is set to zero. A negative value of x_0, away from the limb, results in a negative spike at $x - x_0$ (lower curve), a positive value, closer the solar limb, results in a positive spike. Only in the case when $x = x_0$ the change of function T_s with displacement will be smooth (Lindsey & Roellig 1991).

metric location of such points is reached applying a purely Δx arithmetic offset expressed by $2\Delta x = x_- + x_+$. Thus, this offset applied to the entire raster will align it with the solar disk of the EIT/SOHO image along its tracking direction. This task requires obviously the absence of emission beyond the limb such as that associated with a solar prominence. For this purpose we selected the scan closer to the solar disk diameter.

Seven scans that crossed the solar prominence position showed obvious structure at the east limb (see Figure 2). In the same fashion, data of raster columns were taken to compute symmetry points in the y direction. The mean offsets of the raster were $\Delta x = -1.5$ and $\Delta y = -2$ arcmin.

After the corrections, the middle point of the scan was taken as a *pivot point*, in the sense that the left half of scan was pivoted around it and subtracted from the right side. Applying this to the seven scans involved with the solar prominence, the negative x-axis half was assumed to be the background signal (see Figure 2) and subtracted from the right half. Thus, we obtain the signal of the prominence over the background level.

After obtaining the brightness temperature T_b of the signal excess associated with the solar prominence in both observations, we computed the flux of the peak brightness temperature T_b for each frequency. Calibration of the flux was done using data from the Nobeyama Radioheliograph data[3] which provides the daily mean flux coming from the center of the solar disk in quiet Sun conditions.

4. RESULTS

Seven SST scans passing through the solar prominence for each observation frequency were processed as described previously resulting in 7×21 sub-raster detection points that cover entirely the solar prominence. Figure 5 presents the radio maps at both observing wavelengths created from the data points overlaid over a segment of the 195 Å EIT/SOHO image.

These radio maps reveal an emission structure which has a maximum brightness temperature of 2490 and 2070 K for 1.41 and 0.74 mm, respectively. The maximum brightness temperature in the two observing wavelengths is detected in two quite different regions within the prominence. The peak emission at 1.41 mm is located at $x = 10.7$ arcmin and $y = 15.2$ arcmin and the one at 0.74 mm is located at $x = 11.5$ arcmin and $y = 12.7$ arcmin relative to the solar disk center. Observations by Bastian, Ewell, & Zirin (1993) of a solar prominence at 850 and 1250 μm have shown that the peak emission brightnesses are coincident. However, in their case, the 850 μm emission yields a peak brightness temperature of 615 K, while at 1250 μm the maximum brightness temperature, i.e. 1480 K, that is higher frequencies yield higher peak temperature brightness.

In our observations, the peak brightness temperatures at the two wavelengths are separated by $\sim$4 arcmin with the higher frequency closer to the solar limb. The shapes of the emission region at both frequencies are elongated, with the longest axis aligned with the raster scan direction (see Figure 5) for both observing wavelengths. The ratio of the shortest to the longest axis is 1:3 for the two regions. Even though the maximum temperature brightness is quite similar (differing by $\sim$20%) the emission at 1.41 mm seems to be concentrated within a diameter of 3 arcmin on its long axis, while a similar fraction of the peak emission at 0.74 mm seems to be contained within a diameter of 6 arcmin.

We can estimate the projected height from the limb. This height will be a lower limit since the distance is projected on the sky. The brightness temperature peak at 0.74 mm is at a lower distance (88×10^3 km) than the peak at 1.41 mm (located at a distance of 166×10^3 km).

Table 1 summarizes the prominence observing results for each of the SST observing wavelengths. It

[3] http://solar.nro.nao.ac.jp/norp/data/avg/.

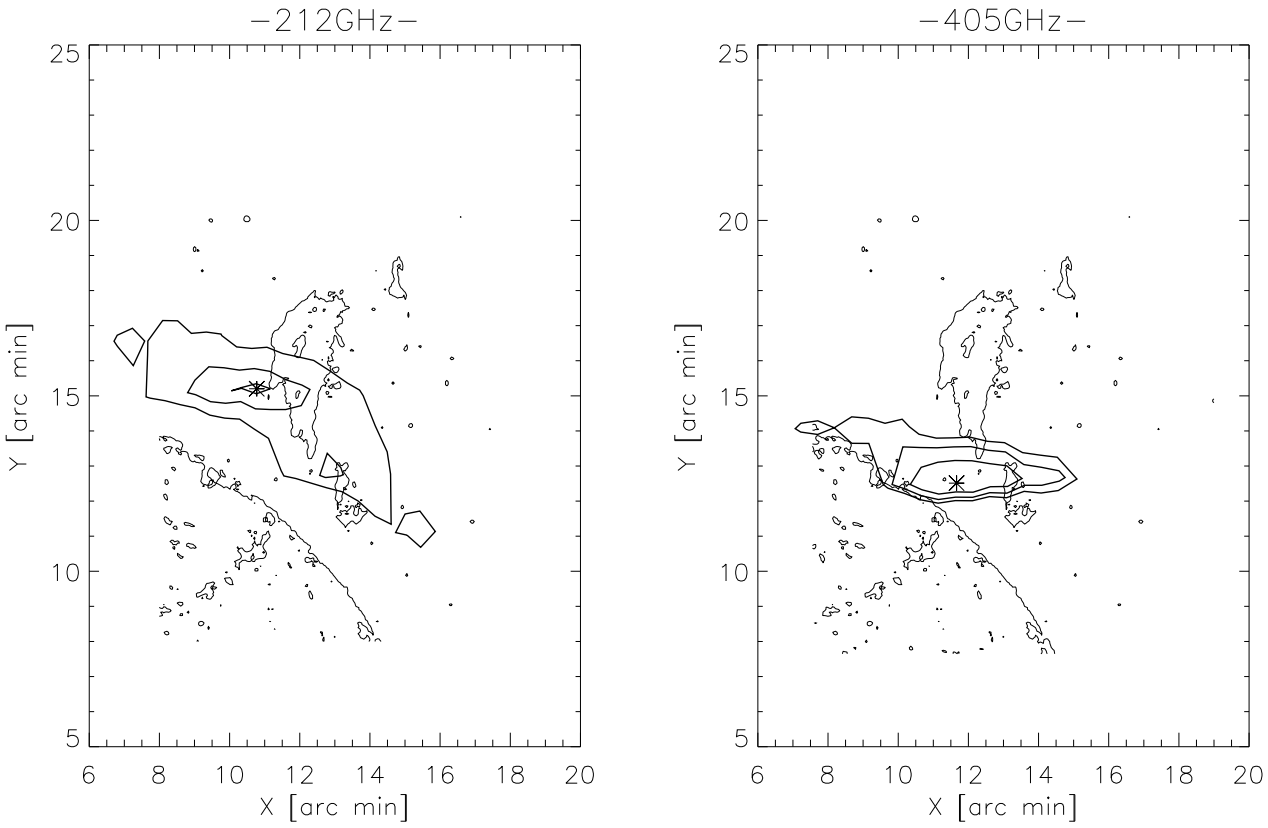

Fig. 5. Radio maps at 212 GHz (λ = 1.41 mm, left panel) and 405 GHz (λ = 0.74 mm, right panel) of the solar prominence on 2009 September 26. Radio maps are presented on a segment of the 195 Å EIT/SOHO image. They were made from a 7×21 raster-scan matrix zoomed on the prominence region. The axes show coordinates relative to the solar disk center in the local horizontal coordinate system. The fitted contours reveal the radio emission structure which peaks in the bottom part of the prominence indicated by an asterisk. The range of contour evaluation for the 212 GHz radio map runs from 909 to 2909 ADC, and for the 405 GHz radio map from 18 to 709 ADC. The positions of the peak emission are at (10.7,15.2) and (11.5,12.7) for the 212 and 405 GHz radio maps respectively. The HPBW are $4'$ for 212 GHz and $2'$ for 405 GHz.

TABLE 1

SOLAR PROMINENCE OBSERVED AND DERIVED PARAMETERS

	Observed			Derived		
Wavelength [mm]	T_b(max)[a] [K]	(Az, El)[b] [arcmin]	h[c] [km]	τ_ν[d]	T_e[e] [K]	n_e[f] [cm^{-3}]
0.74 (405 GHz)	2070	$x = 10.8, y = 11.5$	87×10^3	0.37	5640	9.76×10^9
1.41 (212 GHz	2490	$x = 10.7, y = 15.2$	166×10^3	0.44	5620	9.06×10^9

[a]Maximum observed brightness temperature.

[b]Coordinates of T_b(max) projected position relative to the solar disk center.

[c]Projected height over the solar limb of the brightness temperature peak.

[d]Plasma free-free optical depth at frequency ν.

[e]Plasma electron temperature.

[f]Plasma electron density.

shows the maximum observed brightness temperature, T_b(max), the position of the brightness temperature peak, in arcmin, relative to the solar disk center, and the projected height over the solar limb, h, in kilometers.

From the SST calibration processes, it was found that the receiver noise temperatures during the observing time were 2740 and 4700 K, for the 1.41 and 0.74 mm receiver, respectively. The atmospheric zenith opacity during the observing time was 0.15 and 0.77 for wavelengths of 1.41 and 0.74 mm, respectively. In particular, these values of the submillimetric optical depth of the atmosphere at the observing time favored this successful observation since typical values of the optical depth for El Leoncito site are 0.18 and 0.9 for 1.41 and 0.74 mm, respectively (Melo et al. 2003).

5. DISCUSSION

In § 3 we showed how to subtract the contribution from the Sun and how to deconvolve the telescope response to leave only the signal from the prominence alone. The method was applied to the 1.41 and 0.74 mm raster-scan maps of the solar prominence. The data at both wavelengths were obtained simultaneously, both in space and time, since the receivers' beam footprints are concentric (see Figure 1). In this section we followed the method of Bastian et al. (1993) to derive and discuss the plasma parameters of the observed solar prominence at the two observing wavelengths.

The ionization fraction $n_e/H_{\rm I}$ of a solar prominence is not a well-determined quantity; it can vary from $n_e/H_{\rm I} \approx 0.16$ at the cool part of the prominence (Landman 1986) up to $n_e/H_{\rm I} \sim 1$ at the outer parts (Hirayama 1985). Under these circumstances, electron/ion free-free absorption is the dominant source of opacity at wavelengths near 1 mm. The electron temperature T_p in quiescent prominences is also somewhat uncertain. Zirin (1988) argues that the electron temperature is likely to be in the range 4800–6000 K. Hirayama (1985) has suggested that an average value of 5600 K is appropriate. For the purpose of this discussion, we assume that the prominence temperature is within the range 5000–6500 K. While Hirayama (1964, 1971) has also noted the tendency of prominence temperatures to increase towards their periphery, we assume that the dense core of a prominence is essentially isothermal, an assumption which allows us to treat the observations in a simple manner without introducing a large error.

The observed brightness temperature T_b, without the presence of background emission, is related to the plasma temperature, T_p, by (Dulk 1985)

$$T_b = T_p(1 - e^{-\tau_p}) \,, \tag{6}$$

where τ_p is the optical depth of the material in the prominence. The free-free absorption coefficient, $\kappa_\lambda^{\rm ff}$, that describes the plasma opacity, τ_p, is given by (Lang 1980)

$$\kappa_\lambda^{\rm ff} = 1.089 \times 10^{-23}\, n_e^2\, T_e^{-1.5}\, \lambda^2 \times \log\left(1.652 \times 10^{-3}\, T_e^{1.5}\, \lambda\right) \ {\rm cm}^{-1} \,, \tag{7}$$

where λ is the wavelength in cm, T_e is the effective temperature of the emitting material, and n_e the electron number density. Since

$$\tau_\lambda^{\rm ff} \,=\, \int_0^L k_{\rm ff}\, ds \,=\, f(\lambda, T_e) \langle n_e^2\, L \rangle \ , \tag{8}$$

where L is the physical size along the line of sight and $f(\lambda, T_e)$ a function of λ and T_e, radio observations may help us to constrain the plasma optical depth and, therefore, the average emission measure $\langle n_e^2\, L \rangle$ as a function of the projected position in the prominence.

The peak brightness temperature at 1.41 mm is 2490 K and it is separated by ∼4 arcmin from the maximum at 0.74 mm, where its peak brightness is 2070 K. Free-free emission from solar prominences at millimeter and sub-millimeter wavelengths is optically thin (Bastian et al. 1993), so we assume that both emissions are optically thin. Using equation (7) the maximum brightness of the 1.41 mm prominence emission yields a peak line-of-sight emission measure $\langle n_e^2\, L \rangle = (1.84 - 1.93) \times 10^{29}$ cm^{-5} for T_p in the range of 5000–6500 K. Similarly, the 0.74 mm prominence emission yields $\langle n_e^2\, L \rangle = (6.52 - 6.73) \times 10^{29}$ cm^{-5}. By comparison Bastian et al. (1993) obtained values in the range of $(1.15 - 2.02) \times 10^{29}$ cm^{-5} for 0.85 mm and $(1.26 - 2.30) \times 10^{29}$ cm^{-5} for 1.25 mm for T_p in the same temperature range as before. Thus, the mean optical depth at 0.74 and 1.41 mm will be $\tau_{0.74} = 0.37 \pm 0.05$ and $\tau_{1.41} = 0.44 \pm 0.07$, respectively.

To disentangle the mean electron density from the emission measure we need to make further assumptions. For L, let us assume a path length similar to the projected widths of the most intense cores for each wavelength, i.e. we are assuming a cylindrical emitting region with long axis along the line of sight equal to the cross section of the projected emission core. Thus, for 0.740 mm it will be $L = 6.96 \times 10^4$ km, and for 1.41 mm it will be $L = 2.32 \times 10^4$ km for angular diameters 3 arcmin and 1 arcmin, respectively (see Figure 5). With these

values of L, we obtain the following electron densities for the emitting regions at 0.740 and 1.41 mm of $n_e = 9.76 \times 10^9$ and 9.06×10^9 cm^{-3}, respectively. Assuming an optically thin emission the plasma temperature will be $T_P = 5640$ K for the 0.74 mm emission region and 5620 K for the 1.41 mm emission region.

6. CONCLUSIONS

1. We have analyzed data from the *Solar Submillimeter Telescope* (SST) in raster scan observations mode on 2009 September 26, and found a radio emission structure beyond the solar limb at wavelengths 1.4 and 0.74 mm (212 and 405 GHz, respectively).

2. By comparing these SST scans to images at the chromospheric line of He II (304 Å) from EIT/SOHO instrument properly oriented, we found that the excess of radio emission coincides with the location of a solar prominence at 19:19 hours UT at the SST on 2009 September 26.

3. During the observations, the millimeter zenith atmospheric opacity at the SST site was $\tau_{212} = 0.15$ and $\tau_{405} = 0.77$, much lower than the most probable opacity values for the telescope site. These fortunate circumstance allowed us to detect the solar prominence with a good signal to noise ratio at the submillimeter and millimeter wavelengths.

4. Using geometrical arguments for each scan, and with help of the He II image, we subtracted radio background signal to get a peak brightness temperature of the prominence structure of $T_b = 2490$ and 2070 K for the wavelength emission at 1.4 and 0.74 mm, respectively. The brightness temperature peaks were separated by ∼4 arcmin, with the shortest wavelength being closer to the solar limb.

5. We have applied the free-free mechanism theory developed by Dulk (1985) for the solar disk to the solar prominence at a projected distance of $h \sim 10^5$ km over the solar limb to derive its electronic density and plasma temperature.

6. The emission is consistent with optically free-free radiation, the optical depth being $\tau_{0.74} \approx 0.37$ at the brightness maximum. For the range of temperatures of 5000–6500 K we find that the emission measure lies in the range of $(1.84 - 1.93) \times 10^{29}$ for 1.41 mm and $(6.52 - 6.73) \times 10^{29}$ for 0.74 mm. The electron temperature at both wavelengths is $T_e = 5600$ K.

J. E. Pérez-León thanks Consejo Nacional de Ciencia y Tecnología (Conacyt), Mexico, for a graduate student fellowship. He II solar images are a courtesy of EIT/SOHO consortium. SOHO is a project of international cooperation between ESA and NASA. The SST program is being partially funded by Brazil agencies FAPESP and CNPq and Argentina agency CONICET.

REFERENCES

Apushkinskii, G. P., & Topchilo, N. A. 1985, Soviet Astron., 29, 454
Apushkinskij, G. P., Topchilo, N. A., Tsyganov, A. N., & Nesterov, N. S. 1996, Astron. Nachr., 317, 417
Bastian, T. S., Ewell, M. W., & Zirin, H. 1993, ApJ, 418, 510
Dulk, G. A. 1985, ARA&A, 23, 169
Golubchina, O. A., Bogod, V. M., Korzhavin, A. N., Bursov, N. N., & Tokhchukova, S. Kh. 2009, in ASP Conf. Ser. 405, Solar Polarization 5: In Honor of Jan Olof Stenflo, ed. V. Sveltana, S. V. Berdyugina, K. N. Nagendra, & R. Ramell (San Francisco: ASP), 441
Hirayama, T. 1964, PASJ, 16, 104
_____. 1971, Sol. Phys., 17, 50
_____. 1985, Sol. Phys., 100, 415
Hiriart, D., Goldsmith, P. F., Skrutskie, M. F., & Salas, L. 1997, RevMexAA, 33, 59
Jejčič, S., & Heinzel, P. 2007, in ASP Conf. Ser. 368, The Physics of Chromospheric Plasmas, ed. P. Heinzel, I. Dorotovič, & R. J. Rutten (San Francisco: ASP), 325
Kaufmann, P., et al. 2008, Proc. SPIE, 7012, 70120L
Landman, D. A. 1986, ApJ, 305, 546
Lang, K. R. 1980, Astrophysical Formulae (2d ed.; Berlin: Springer)
Lantos, P., & Raoult, A. 1980, Sol. Phys., 66, 275
Lindsey, C. A., & Roellig, T. L. 1991, ApJ, 375, 414
Melo, A. M., et al. 2003, Bol. Sociedade Astronômica Brasileira, 23, 202
Otárola, A., Hiriart, D., & Pérez-León, J. E. 2009, RevMexAA, 45, 161
Silva, A. V. R., et al. 2005, Sol. Phys., 227, 265
Wild, J. P., & Zirin, H. 1956, Aust. J. Phys., 9, 315
Zirin, H. 1988, Astrophysics of the Sun (Cambridge: Cambridge Univ. Press)

J. E. Pérez-León and D. Hiriart: Instituto de Astronomía, Observatorio Astronómico Nacional, Universidad Nacional Autónoma de México, Apdo. Postal 877, Ensenada, B. C., 22800, Mexico (eperez, hiriart@astrosen.unam.mx).
J. E. Mendoza-Torres: Instituto Nacional de Astrofísica, Óptica y Electrónica, Luis Enrique Erro, 1, Tonantzintla, Puebla, 72840, Mexico (mend@inaoep.mx).